Numerical study of novel air-based PVT designs validated using standardized testing approach.

Giorgos Aspetakis[1], Qian Wang[1,2]

[1] Department of Civil and Architectural Engineering, KTH Royal Institute of Technology, Teknikringen 78, Stockholm, 114 28, Sweden

[2] Uponor AB, Hackstavägen 1, Västerås, 721 32, Sweden

Abstract

The study focuses on the simulation of a novel Air-Based Photovoltaic Thermal (PVT) prototype, experimentally investigated according to ISO 9806, specifically for collectors generating thermal and electrical energy. Experimental studies are carried out to validate a benchmark Computational Fluid Dynamics (CFD) simulation model in a previous study. The same setup shall be used to explore new thermal enhancement designs of the prototype. The aim of the model is on the one hand to assess the thermal performance enhancement of multiple newly developed inserts/baffles. The results indicate the optimal design selections for next-step experimental prototypes. The secondary objective is to assess the feasibilities of the PVT prototype for operational characteristics at different climate conditions. Insights are provided regarding the reliability, workflow and overall methodology of validating CFD models by testing through an international standardized process. Outlines for system-level modelling are presented as well.

Keywords: PVT, simulation, experimental, validation

1. Introduction

Building integrated PVT solutions have shown promising potential for covering thermal and electrical demand in residential applications. However, the efficiency of photovoltaic cells drops linearly with temperature (Skoplaki and Palyvos, 2009). Cooling PV modules effectively enhances their electrical efficiency and prolongs their operational lifetime (Dwivedi et al., 2020). Decentralized on-site renewable energy generation in forms of both thermal and electrical energy is vital for the transition to a carbon free society. PVTs can assist in facilitating sustainable growth worldwide and are strongly linked to the UN's Sustainable development goals 7 and 11 which focus on clean, affordable energy production and sustainable cities respectively.

By cooling PV modules, PVT systems can maintain increased electrical efficiency and generate thermal energy. Waste heat from the PV surface causes a temperature rise of the cooling medium which can subsequently be harnessed. Air based systems, frequently overlooked, are examined in this study. Such systems require testing and experimental studies to validate for numerical simulations and/or to evaluate real-life performance. To develop thermally efficient designs, Computational Fluid Dynamic (CFD) models can evaluate the performance of different insert arrangements, in only a fraction of time and effort of a fully-fledged outdoor testing sequence. Therefore, to uphold credible results, a validation process has already taken place.

Scaling up solutions is equally important for the wide-adoptions of PVT technology. The feasibility of scaled up configurations can be estimated by utilizing simulations of PVT systems, for example, CFD or analytic numerical ones, without experimentally testing each individual case. To further strength the replicability and scalability, standardized testing approaches were utilized. Current literature investigated various designs, yet few studies carry out validations based on standard approach.

Testing in regions with low solar potential, such as the Nordic countries, is of also of great interest, with limited studies available. In the current study, validation data are obtained from standardized testing of a blank channel PVT collector located in Sweden.

The test methods described in the ISO 9806:2017 (*ISO 9806:2017 Solar energy — Solar thermal collectors — Test methods*, 2017) standard are applied for certifying solar thermal collectors, including a dedicated part for thermal performance evaluation. The enhanced thermal performance of a newly developed PVT configuration, with a blank

10.18086/swc.2023.03.02 Available at http://proceedings.ises.org

air-channel, has been selected following the ISO 9806 testing procedure. The intent of this study is to present reliable designs, which have been developed using validated CFD models. More specifically, the aim is to determine the necessary requirements for successful CFD simulation of Air-based PVT collectors. These are incorporated in general guidelines for researchers and engineers that might have ISO test report.

2. Methods

2.1 Experimental testing

ISO 9806:2017 (ISO 9806:2017 Solar energy — Solar thermal collectors — Test methods, 2017) was followed for testing the thermal performance of the PVT prototype. A subsection is addressed to co-generating collectors. PVTs can therefore be tested with the same methods as solar air heaters, at the electrical maximum power point of the solar cells. More specifically, the prototype fits under the categories of air-heating collectors and Wind or Infrared Sensitive Collector (WISC), because the cooling medium utilized is air and the absorber surface, in this case the PV modules, are exposed to the ambient with no glazing.

An experimental testing rig located in in central Sweden was built for measurements. On a fixed angle base, situated on ground level a prototype PVT system was installed, consisting of PV panel, cooling channel underneath panel, air ducts, air fan unit and measurement instruments. The open-to-ambient configuration without air preconditioning, described in the standard, was implemented, shown in Figure 1. Ambient air is circulated through a blank channel under the PV surface through negative pressure. The standard requires temperature measurements with a maximum uncertainty of 0.2 K, thus Pt-100 RTD sensors were selected. For flow measurements, it was stressed that the sensor should not utilize thermal measurement methods. Therefore a configuration of a differential pressure transducer coupled with a Pitot tube was set up, from which the volume flow is calculated. The same pressure transducer was utilized to measure the pressure drop of the PVT

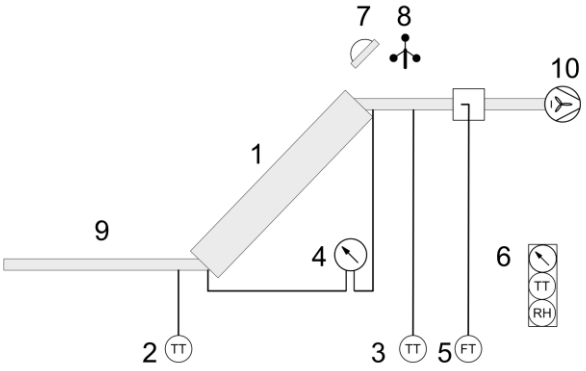

1. PVT Collector
2. Inlet Temperature
3. Outlet Temperature
4. Differential Pressure
5. Flow Meter
6. Ambient Measurement
7. Pyranometer
8. Anemometer
9. Air Duct
10. Fan

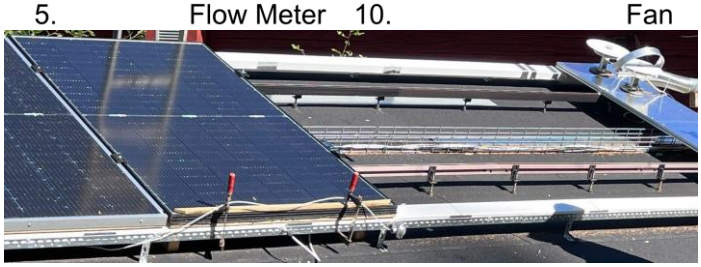

Fig. 1: Open-to-ambient setup with listed sensors and photo of the installation.

prototype. Two pyranometers were installed parallel to the PVT surface for global and diffuse irradiance monitoring, respectively. Alongside those, a cup anemometer was placed for measuring the wind parallel to the surface, in order to assess its effect on performance. Maximum Power Point Tracking (MPPT) was achieved through an inverter connected to the electrical output of the panel, measuring simultaneously the power output in real time. All data flows were directed to a central datalogger system. An example of measured data is presented in Figure 2, in which shows the inlet and outlet temperatures of the collector for a typical summer day.

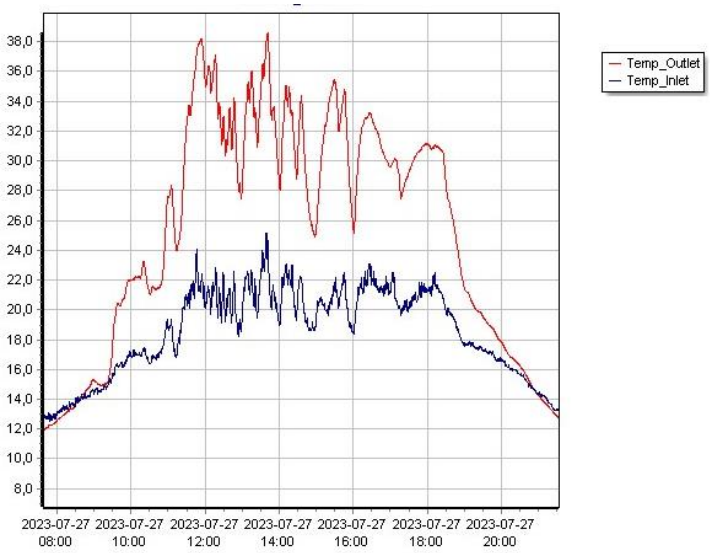

Fig. 2: Temperature of collector inlet and outlet for a typical summer day.

Table 1 presents the specifications of testing instruments measuring instruments along with their accuracy ranges. As per the standard, irradiance levels are always higher than 700 W/m^2 and near normal incidence angles were tested.

Tab. 1: Measuring instruments utilized in the experiment, detailing measurement location, type of sensor, brand and accuracy.

Measurement	Location	Type	Sensor	Accuracy
Temperature	Inlet Flow/Ambient	Pt-100 RTD	JUMO Etemp	±(0,1+0,0017 * T) K
	Outlet Flow			
Mass flow	Outlet Flow	Diff. Pressure+ Pitot Tube	KIMO CP212-HO-R	±0.5% of reading ± 2 Pa
Irradiance	Parallel to PV Surface	Pyranometer	Kipp & Zonen CM11	±2%
PV Electrical	PV Output	Inverter	In-house built	±1%
Windspeed	Parallel to PV Surface	Cup Anemometer	Thies Clima WT	±0.5 m/s
Datalogger	-	-	Campbell CR1000X	±(0.04% of reading + offset)

Validation of simulation models in Sola Air Heaters and PVT technologies typically requires the characterization of thermodynamic and hydraulic performance, which respectively necessitate the calculation of the Nusselt number (Nu) and friction factor for different Reynolds numbers (Re). Thus, measurements are taken at multiple flowrates and consequently at different Re values. The standard testing requires measurements at 3 mass flow rates. In this testing instance, these are expanded to 5 in order to incorporate the validation process in the standardized testing sequence. Effectively, two functions are served with one testing routine. Testing blocks had a duration 20 minutes allowing for stabilization of monitored values.

2.2 Calculations

For calculating thermal power output, measured physical quantities of the airflow are used. The temperature rise of the airflow underneath the PV surface caused by the exposure to solar irradiance is described below,

$$q_{col} = \dot{m}C_p(T_{out} - T_{in}) \quad \text{(eq. 1)}$$

The heat transfer to the working fluid through convection is

$$q_{conv} = h(\bar{T}_{sur} - T_b) \quad \text{(eq. 2)}$$

Where T_{sur} is the average surface temperature and

$$T_b = \frac{T_{out}+T_{in}}{2} \quad \text{(eq. 3)}$$

which corresponds to the power output of the collector. Thus

$$q_{col} = q_{conv} \rightarrow h = \frac{\dot{m}C_p(T_{out}-T_{in})}{(\bar{T}_{sur}-\frac{T_{out}+T_{in}}{2})} \quad \text{(eq. 4)}$$

The Nusselt number describes the ratio of convective to conductive heat transfer at a boundary in a fluid in the following way

$$Nu = \frac{hD_H}{k} \quad \text{(eq. 5)}$$

And the friction factor *f* is a dimensionless number characterizing the energy needed to overcome the induced pressure drop.

$$f = \frac{(\Delta P/L)D_H}{2\rho U^2} \quad \text{(eq. 6)}$$

The needed variables are measured and calculated from the testing, at different mass flow rates that lead to different Reynolds numbers:

$$Re = \frac{UD_H}{\nu} \quad \text{(eq. 7)}$$

Where

$$D_H = \frac{4\times Area}{Wetted\ Perimeter} \quad \text{(eq. 8)}$$

is the hydraulic diameter.

2.3 Simulation

ANSYS Fluent was applied for numerical calculations. Li et al. investigated the performance of various turbulence models in transpired collector applications and showed that the K-epsilon RNG turbulence model delivered the highest accuracy and consistency, with low computational demand. In this study, given the highly similarity of the heat transfer in PVT collectors and transpired collectors, this particular turbulence model was selected. Turbulent intensity was assumed to be around 5%. The interior walls of the collector are considered are set to no-slip condition and adiabatic due to the insulation installed. Since the heat transfer between surface and airflow needs to be investigated, the thermal boundary layer must be solved, requiring thus a value of y^+=1. The mesh has therefore been constructed accordingly and is shown in Figure 3.

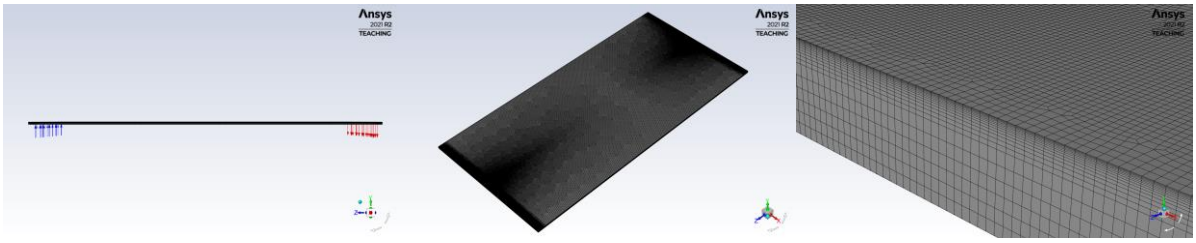

Fig. 3: Mesh of the CFD model, additionally showing applied inflation and inlet/outlet boundary.

To ensure the validity of the results, convergence criteria were set to 10e-6, and for the energy equation 10e-9. The boundary conditions were set according to experimental values. These include: irradiance, inlet temperature equal to ambient, flowrate, surface temperature. At the inlet a mass flow inlet was set, pressure outflow at the exit. At the wall surfaces, adiabatic heat flux boundary conditions were set. For the PV surface the following heat balance holds:

$$q = \alpha G - \varepsilon\sigma(T_{sur}^4 - T_\infty^4) - h(T_{sur} - T_a) - {}^{P}/_{A} \qquad \text{(eq. 9)}$$

Where α is the absorptance, ε emittance, σ Stefan-Boltzmann constant, h the heat transfer coefficient and P the electrical power generated. The terms in respective order represent the heat transferred to the airflow, absorbed solar irradiance, radiation losses, convection losses and electrical power generated. A diagram of the heat balance is shown in Fig 4.

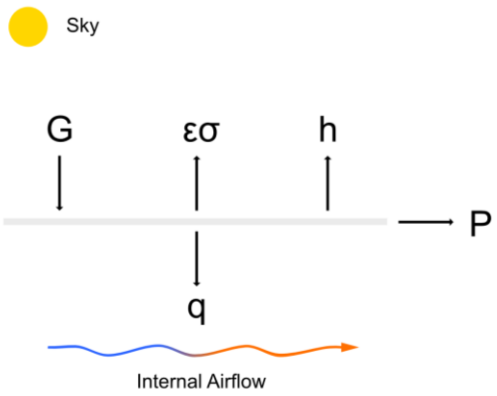

Fig. 4: Illustration of heat transfer at the PV surface boundary.

For the convection, the correlations for the heat transfer coefficient of solar collector cover glass developed by (Watmuff et al.,1977) have been utilized.

$$h_{glass} = 2.8 + 3u_{wind} \qquad \text{(eq. 10)}$$

The radiation temperature was calculated in a similar study (Kim et al., 2020) and is derived from:

$$T_\infty = 0.00552T_a^{1.5} \qquad \text{(eq. 11)}$$

Thus a mixed boundary condition can be used. Table 2 describes the different boundary conditions set in the simulation model.

Tab. 2: Location and Source of Boundary Conditions

Test Data Source	CFD Boundary Condition	Location
Irradiance G	Heat flux	PV Surface
Ambient Temp	Inlet Temperature	Inlet
Flowrate	Mass flow inlet	Inlet
-	Pressure Outflow	Outlet
-	Adiabatic	Walls

3. Results and Discussions

A comparison of test and simulated average outlet temperature is shown in Fig 5. Good agreement between results is achieved. Particularly, mean absolute error (MAE) is calculated 0.25 °C and normalized root square mean error (NRMSD) at 1.07%. Outlet temperature drops with higher mass flows. A slight increase is observed at 0.03 kg/s due to elevated irradiance levels at the time of testing, as shown in Fig. 5.

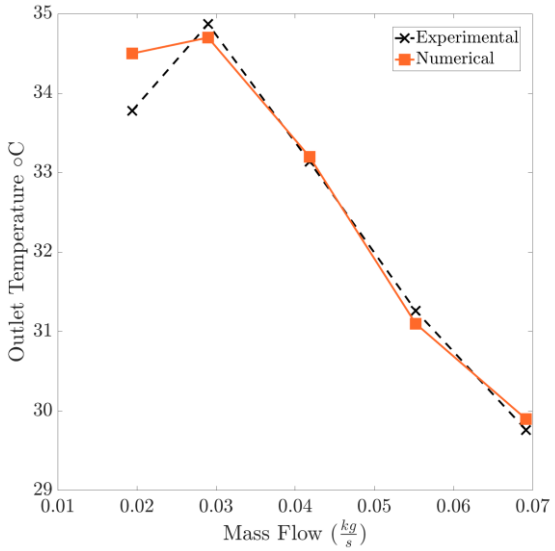

Fig. 5: Experimental and numerical outlet Temperature for different mass flows.

In Figure 6, the comparison of test and simulated thermal output is presented and displays acceptable agreement. MAE is equal to 8.44 W and NRMSD to 7.7%. Heat generated rises with mass flow rate. Although outlet temperature has decreased, a greater amount of air has been heated which translates to higher heat output. However, to achieve higher mass

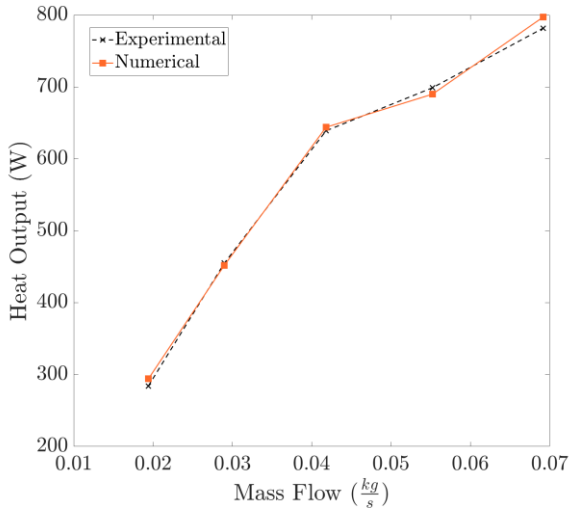

Fig. 6: Experimental and numerical thermal output for different mass flows

flows, blowers are required to compensate with higher pressure drops. The correlation is illustrated in Figure 7 where pressure drops measured and simulated are displayed. As expected, pressure drop increases with mass flow. Good agreement is observed, with higher mass flows containing relatively larger error. MAE was calculated at 1.38 Pa and NRMSD 17.1%. This might be due to the effect of minor losses and entrance effects which are under a quadratic correlation to the velocity of the flow, notably 90° turns and change of hydraulic diameter.

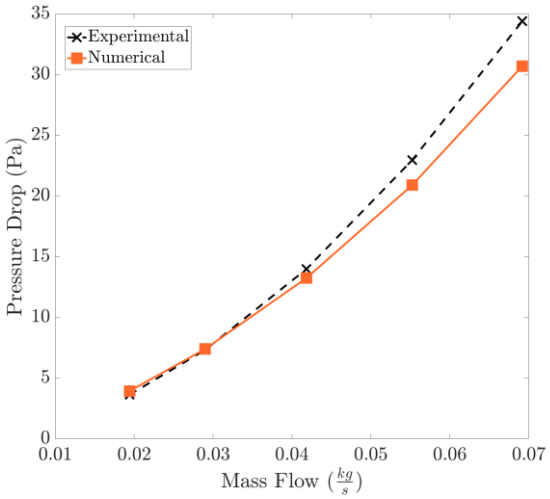

Fig. 7: Experimental and numerical pressure drop for different mass flows.

The Nusselt no. for different Reynolds no. values are displayed in Figure 8. Nu increases as the flow becomes more turbulent, as expected. Yet it remains relatively low, indicating that room for improvement exists. Various techniques have been developed on this front, most notably thermal inserts or modified absorber surfaces. As introduced, those add friction to the flow causing greater pressure drops. This effect is expressed by the friction factor *f*, presented in Figure 9. These values are expected to rise when thermal inserts are added. Designs that cause lower friction increase play an essential role in this application.

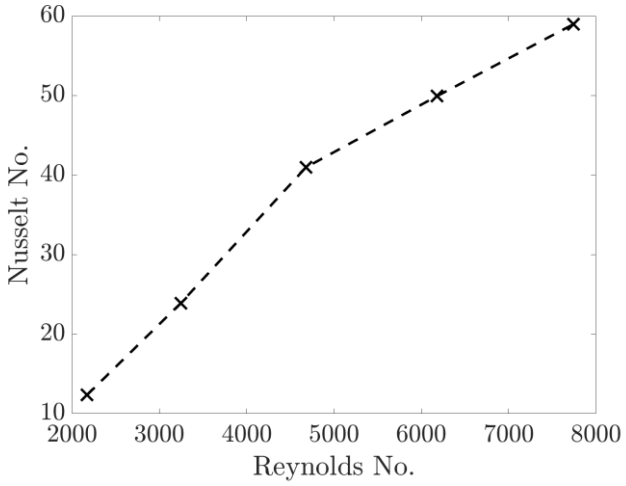

Fig. 8: Numerical Nusselt no. for different Reynolds no.

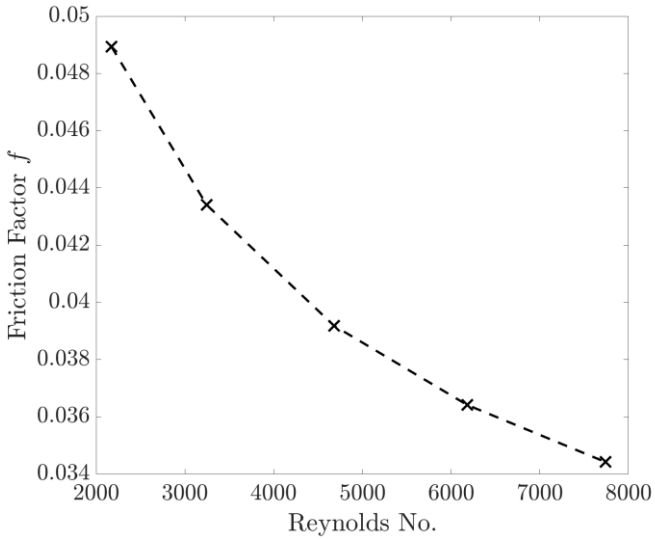

Fig. 9: Numerical Friction Factor f for different Reynolds no.

The results of the CFD simulation agree with test measurements, both in terms of thermal and pressure aspects, indicating that the CFD model can be considered valid for future investigations, having been validated by field testing. Thus, measurements according to ISO 9806 are adequate for constructing a CFD model of the collector. The necessary inputs can be derived from the ISO 9806 thermal performance report, an example shown in Figure 10. This, combined with corresponding schematics or drawings enables the modelling of collectors that have already been tested using the standardized method of ISO 9806, without performing other measurements. In essence, the measurements performed in the ISO 9806 are adequate for creating and validating a CFD simulation model of the investigated collector. Avoiding the reiteration of testing for older collectors saves a significant amount of time and resources.

Data point	$\dot{m}_i$	G''	ϑ_a	u	$K_b(\theta_T, \theta_L)$	$\eta_{hem,\dot{m}_i}$	$b_{u,\dot{m}_i}$	$\dot{Q}$	Standard deviation
	kg/h	W/m^2	°C	m/s	—	—	s/m	W	W
1									
2									
...									
27									

Fig. 10: Thermal performance report of the ISO 9806 standard, with the utilized parameters highlighted.

Research with streamlined modelling process is better able to explore additional modifications. These potentially lead to the development of new heat transfer enhancements that are suitable either for solar air heating or PVT technologies such as absorber geometries or thermal inserts. The main finding of the current study indicates that CFD modelling sourced with ISO 9806 performance data is a feasible practice.

4. Conclusion

The ISO 9806 standard was followed for the experimental testing of a PVT collector. Based on the measurements, a computational fluid dynamics model was devised. Agreement of experimental and numerical results indicates correct validation of the model. It was noted that the data measured was sufficient to determine the correct boundary conditions needed for the numerical analysis. Thus, investigators in possession of a ISO 9806 thermal performance report and schematics of the collector geometry, are able to successfully simulate thermal collectors or PVTs. As such, novel performance enhancing methods can be further explored with extensive design variations at the early design stage.

5. Acknowledgments

The authors gratefully acknowledge the financial support from the Swedish Energy Agency (grant number: 52488-1).

6. References

Dwivedi, P., Sudhakar, K., Soni, A., Solomin, E., Kirpichnikova, I., 2020. Advanced cooling techniques of P.V. modules: A state of art. Case Studies in Thermal Engineering 21. https://doi.org/10.1016/j.csite.2020.100674

ISO 9806:2017 Solar energy — Solar thermal collectors — Test methods, 2017. International Organization for Standardization, Geneva, Switzerland.

Kim, Y., Lee, K., Yang, L., Entchev, E., Kang, E., Lee, E., 2020. Validation and Numerical Sensitivity Study of Air Baffle Photovoltaic-Thermal Module. Energies 2020, Vol. 13, Page 1990 https://doi.org/10.3390/EN13081990

Li, S., Karava, P., Savory, E., Lin, W.E., 2013. Airflow and thermal analysis of flat and corrugated unglazed transpired solar collectors. Solar Energy 91, 297–315. https://doi.org/10.1016/J.SOLENER.2013.01.028

Skoplaki, E., Palyvos, J.A., 2009. On the temperature dependence of photovoltaic module electrical performance: A review of efficiency/power correlations. Solar Energy 83, 614–624. https://doi.org/10.1016/J.SOLENER.2008.10.008

Watmuff, J., Charters, W., Proctor, D., 1977. Solar and wind induced external coefficients - Solar collectors. Cooperation Mediterraneenne pour l'Energie Solaire, 56

NOMENCLATURE AND SYMBOLS

Quantity	Symbol	Unit
Heat transfer coefficient	h	W m^{-2} K^{-1}
Thermal conductivity	k	W m^{-1} K^{-1}
Hydraulic diameter	D_H	m
Pressure drop	ΔP	Pa
Density	ρ	kg m^{-3}
Flow velocity	U	m s^{-1}
Friction Factor	f	
Reynolds No.	Re	
Nusselt No.	Nu	
Irradiance	G	W m^{-2}
Emittance	ε	
Absorptance	α	
Stefan-Boltzmann constant	σ	W m^{-2} K^{-4}
Heat flux	q	W m^{-2}
Mass flow rate	$\dot{m}$	kg s^{-1}
Specific heat	c	J kg^{-1} K^{-1}
Kinematic viscosity	v	m^2 s^{-1}
Mean Absolute Error	MAE	
Normalized Root Mean Square Error	$NRMSE$	